www.rericjournal.ait.ac.th

Numerical Study of Performance of a Late Mixing Porous Burner (LMPB) for Combustion of Low-Calorific Synthetic-gas from Biomass Gasification

Kanokkarn Jirakulsomchok*,[1] and Sumol Sae-Heng Pisitsungkakarn*

Abstract – *This work examines the performance of a late mixing porous burner (LMPB) in term of radiant output efficiency. The low-calorific-synthetic-gas from Mangium tree gasification was used as a fuel. The system consists of two main porous media: the first one serves as a fuel preheated porous and the second one serve as a combustor that is around with the air jacket for air preheating and preventing heat loss to the surrounding. The two porous media are separated by the small space which serve as a mixing chamber. The study results indicated that the stabilized combustion of low-calorific-synthetic-gas can be occurred. The radiant output efficiency is increased with increasing equivalence ratio while the radiant output efficiency is decreased with increasing firing rate. Moreover, the LMPB provide the radiant output efficiency in the range of 28.5% to 67%.*

Keywords – *biomass, burner performance, combustion, gasification, porous burner.*

1. INTRODUCTION

Biomass is the only renewable energy source, which can store solar energy in the chemical bond during its growth. The stored chemical energy can be utilized by way of thermochemical conversion of biomass. Biomass is an environment-friendly biofuel because it can reduce CO_2 greenhouse effect. Biomass provide characterizations of neutral carbon fixed by photosynthesis during it growth and less sulphur and nitrogen contents [1]-[3]. Among renewable energy *i.e.* solar, wind and biomass energy, biomass is adjustable and controllable energy by amount of supply while wind and solar energy supply is low. Moreover, biomass is available at every place all over the world while coal and natural gas deposits in somewhere in some countries [4]. Therefore, utilization of biomass for alternatives energy is one of the main concerns of governments and many papers were reported to review the status of biomass utilization [5]-[11].

Gasification is one of technologies that converts biomass to combustible gaseous. It provides a high flexibility in using variety of feedstock material. The chemical energy in biomass can be converted by gasification into syngas. The main compositions of syngas are hydrogen, carbon monoxide, carbon dioxide, methane and nitrogen. However, the high inert content in synthetic gas (N_2 and CO_2) results in low heating value and decreasing in the flame temperature and the burning velocity. The stabilization combustion is difficultly occurred in the conventional burner. The super adiabatic combustion process under excess enthalpy burning. The borrowing enthalpy from the combustion products to preheat the incoming reactants result in flame temperature and burning velocity greater than the corresponding adiabatic flame temperature and laminar burning velocity. In this way, the extending lean flammability and low emission combustion can be achieved [12]. One common method of heat recirculating combustor is a burner with heat exchanger (*e.g.*, a counter current heat exchanger, a spiral design for the inlet and outlets with heat transport through the walls from the hot products to the reactants, *etc.*) [13]. An alternative to achieve excess enthalpy combustion is a porous burner with superior heat transfer properties. The combustion within a porous burner provides internal heat recirculation by its structure. The reaction occurs within the cavities of a porous matrix. The recirculating heat from the hot exhaust gas to the incoming fresh mixture is done by solid to solid conduction and radiation of porous structure. An external heat exchanger surrounding the combustor is unnecessary. Many researches indicated that the stabilized combustion of very low-calorific value fuels (*e.g.*, landfill gas, syngas from waste pyrolysis, synthetic gas from biomass gasification, *etc.*) was achieved by using porous burner [14]-[17].

Almost all of aforementioned studies focused on combustion of simulated gas mixture within bi-layer porous burner. A few studies were reported combustion of producer gas generated from biomass gasification. Al-attab *et al.* [18] proposed an experimental study of a small scale biomass fuelled porous media burner with heat recovery unit. Downdraft gasifier and two layers of different diameter alumina balls were used in this experiment. The results indicated that the stabilized submerged flame with low emission both CO and NOx of fluctuation in producer gas composition during the operation can be occurred.

Although the bi-layer porous burner is commonly used in recently researches it has only single preheat zone (*i.e.* in the first porous section). The combustion of low-calorific value synthetic gas from biomass gasification within a late mixing porous burner (LMPB) which have advantages over bi-layer porous burner have not been reported. The LMPB has three preheat zones,

*Combustion Technology and Alternative Energy Research Center – CTAE, Department of Power Engineering Technology, College of Industrial Technology, King Mongkut's University of Technology North Bangkok (KMUTNB), Thailand.

[1]Corresponding author:
Tel: +662 555-2000 ext 6427, Fax: +66 2 555-2000 ext 6427.
Email: kanokkarn.j@cit.kmutnb.ac.th.

i.e. a fuel-preheating zone in the FP, the air-preheating zone in the air jacket and the mixture-preheating zone in the preflame zone in the PC while the conventional premixed porous burner has only single preheat zone in the preflame zone. This is lead to the LMPB provide higher heat recirculation efficiency and higher radiant output efficiency when compared with the conventional porous burner [19]-[21].

The objective of this study is to investigate combustion of low-calorific-synthetic-gas from Mangium tree within a LMPB by mean of numerical modelling. Mangium tree (or Krathin-thepha) is fast-growing tree and can be planted in every area of Thailand. It has high potential serve as an alternative fuel in the future. A single-step global reaction, a one-dimensional model and steady state approach were considered. The thermal structure, effect of equivalence ratio and the firing rate were reported. Moreover, the burner performance in term of the radiant output efficiency was clarified. The results of this work can be used as a basic information for future experimental study.

2. NUMERICAL MODEL

Figures 1 and 2 show the computational domain and the experimental apparatus of LMPB respectively [20]-[21]. The system consists of two main porous media. The first porous is fuel preheated porous (FP) and the second one is porous combustor (PC) is enclosed with the air jacket. The FP is made of a stack of metallic wire screens are packed inside a stainless steel tube of 75 mm in length while the PC is a packed bed of spherical alumina oxide ceramic (with a diameter of 10 mm) randomly packed within a stainless steel tube of 160 mm in length. The steady state condition is considered in this model. A low-calorific-synthetic-gas from biomass gasification flows into the FP at Section 1 and is preheated by hot FP. Suddenly, the combustion air flows through an annular air jacket at Section 4, and is preheated by the hot wall of PC. The preheated fuel and preheated air are mix in the mixing chamber that is a small space between FP and PC. Then the homogeneous preheated fuel-air mixture at T_{mix} flow through the PC and combustion occurs. The FP and the PC are in contact by radiation. Both upstream and downstream ends of the system are exposed to the black surroundings maintained at ambient temperature providing incident radiation $I_0^+\left(\tau_{-x_{FP}}\right)$ at Section 1 and $I_0^-\left(\tau_{x_{PC}}\right)$ at Section 4, respectively. Because of three preheating zone concept of LMPB *i.e.* the fuel preheating zone in FP, the air preheating zone in air jacket and the mixture preheating zone in the upstream zone of PC, the stable combustion of low-calorific-synthetic-gas can be occurred.

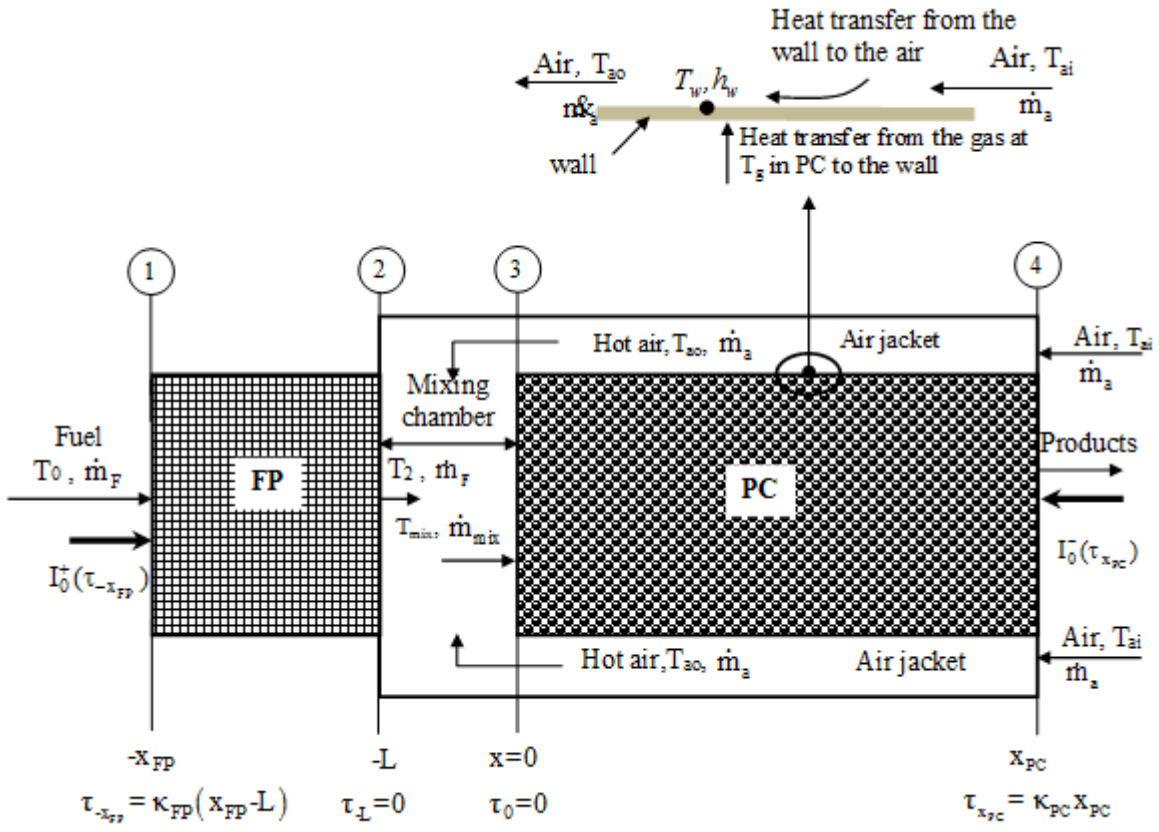

Fig. 1. The computational domain.

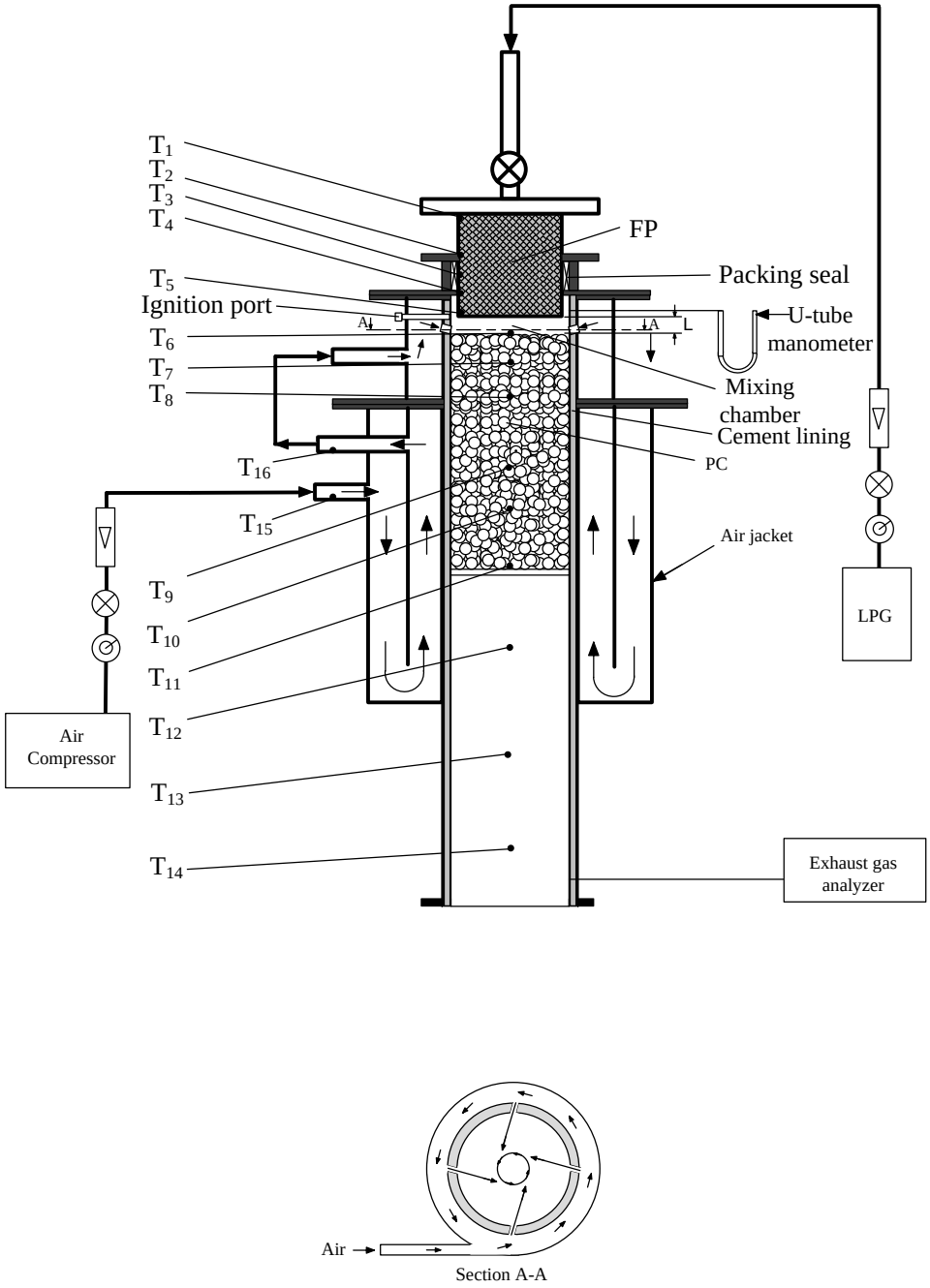

Fig. 2. The experimental apparatus.

The gas and solid conduction, solid radiation, gas convection and the heat transfer between the solid and gas phase are considered in the model. One-dimensional model, a single-step global reaction and a steady state approach are considered in this work. The species and energy conservation equation both in FP and PC are discretized by finite differential approximations. An implicit difference scheme is utilized with respect to time, and a central difference scheme is utilized with respect of space. The convergence criteria of all variables for numerical computation are set to 10^{-6}. The final error in the energy balance is less than 1%.

2.1 Basic Equations

Steady state, 1-D, adiabatic process and incompressible flow condition are considered in this work. Working gas behaves as an ideal gases and is non-radiating. Porous media are inert and able to emit and absorb thermal radiation in local thermal equilibrium, while radiative scattering is ignored**.** The physical properties are constant and the Lewis number is unity (the heat and mass simultaneously transfer by convection). The governing equations are given below [21].

In the FP section, $-x_{FP} \le x \le -L$ $\left(\tau_{-x_{FP}} \le \tau \le \tau_{-L}\right)$, the conservation equations for energy of gas and solid phase are as follow.

$$\rho_F c_F \varepsilon_{FP} \frac{\partial T_F}{\partial t} + \rho_F u_F c_F \varepsilon_{FP} \frac{\partial T_F}{\partial x} = \lambda_F \varepsilon_{FP} \frac{\partial^2 T_F}{\partial x^2} - h_v (T_F - T_s), \quad (1)$$

$$\rho_s c_s (1-\varepsilon_{FP})\frac{\partial T_s}{\partial t} = \lambda_e \frac{\partial^2 T_s}{\partial x^2} - \frac{\partial q_r^n}{\partial x} + h_v (T_F - T_s) \tag{2}$$

The mechanisms of hydrocarbon thermal cracking are negligible in FP, where the local net radiative heat flux within the FP is expressed as: $q_r^{\,n}(\tau) = q_r^{\,+}(\tau) + q_r^{\,-}(\tau)$,

$$q_r^{\,+}(\tau) = 2\pi\left[\begin{array}{l} I_0^+(\tau_{-x_{FP}})E_3\left(\tau_{-x_{FP}} - \tau\right) \\ + \int_{\tau_{-x_{FP}}}^{\tau} I_b(\tau')E_2(\tau' - \tau)\,d\tau \end{array}\right] \tag{3}$$

and

$$q_r^{\,-}(\tau) = -2\pi\left[\begin{array}{l} I_0^-(\tau_{x_{PC}})E_3\left(\tau_{x_{PC}}\right) \\ + \int_{0}^{\tau_{x_{PC}}} I_b(\tau')E_2(\tau')\,d\tau' \end{array}\right] E_3(\tau) - 2\pi\left[\int_{\tau}^{\tau_{-L}} I_b(\tau')E_2(\tau - \tau')\,d\tau'\right]. \tag{4}$$

The optical thickness in the FP section is defined as $\tau = \kappa_{FP}(-L - x)$. The divergence of net radiative heat flux, $\frac{\partial q_r^n(\tau)}{\partial x}$ in Equation 2, is evaluated from the integration of the radiant flux from each part of the porous media FP and PC, and is expressed as:

$$\frac{\partial q_r^n(\tau)}{\partial x} = -2\kappa_{FP}\pi\left[\begin{array}{l} -2I_b(\tau) \\ + \int_{\tau_{-x_{FP}}}^{\tau_{-L}} I_b(\tau')E_1\left(|\tau - \tau'|\right)d\tau' \\ + I_0^+\left(\tau_{-x_{FP}}\right)E_2\left(\tau_{-x_{FP}} - \tau\right) \end{array}\right] - 2\kappa_{FP}\pi\left[\begin{array}{l} I_0^-\left(\tau_{x_{PC}}\right)E_3\left(\tau_{x_{PC}}\right) \\ + \int_{0}^{\tau_{x_{PC}}} I_b(\tau')E_2(\tau')\,d\tau' \end{array}\right] E_2(\tau)\,. \tag{5}$$

Where,

$$I_b(\tau) = \frac{\sigma T_s^4(\tau)}{\pi}$$

$$\int_{\tau_{-x_{FP}}}^{\tau_{-L}} I_b(\tau')E_1\left(|\tau - \tau'|\right)d\tau' = \int_{\tau_{-x_{FP}}}^{\tau} I_b(\tau')E_1(\tau' - \tau)\,d\tau' + \int_{\tau}^{\tau_{-L}} I_b(\tau')E_1(\tau - \tau')\,d\tau'$$

and $E_n(\tau) = \int_0^1 \eta^{n-2} e^{-\tau/\eta}\,d\eta$, n = 1, 2, 3.

In the mixing chamber, the conservation equations for mass and energy are given by:

$$\dot{m}_{mix} = \dot{m}_F + \dot{m}_a, \text{ and} \tag{6}$$

$$\dot{m}_{mix} h_{mix}(T_{mix}) = \dot{m}_F h_F(T_2) + \dot{m}_a h_a(T_{ao}) \tag{7}$$

The mixture of fuel and air at temperature T_{mix} is completely premixed as it enters the PC at Section 3.

In the PC section, $0 \le x \le x_{PC}$ $\left(\tau_0 \le \tau \le \tau_{x_{PC}}\right)$

Gas phase energy equation:

$$\rho_g c_g \varepsilon_{PC}\frac{\partial T_g}{\partial t} + \rho_g u_g c_g \varepsilon_{PC}\frac{\partial T_g}{\partial x} = \lambda_g \varepsilon_{PC}\frac{\partial^2 T_g}{\partial x^2} + \varepsilon_{PC} h_o w - h_v(T_g - T_s) - \alpha U_w\left(T_g - T_w\right). \tag{8}$$

Because of good thermal conductivity of the wall, the PC wall temperature is assumed constant at T_w. The last term on the right-hand side of Equation 8 is heat transfer from the hot gas in PC to the wall, which preheats the air flowing in the air jacket. The reaction rate is considered to follow the first-order Arrhenius equation,

$$w = A\rho(1-y)e^{-E/RT} \tag{9}$$

Moreover, based on the experimental results, peak temperatures are observed within the region of the PC. This indicates that main combustion is taken place inside the PC. Therefore, reaction is assumed to start and get completed only in the PC.

The conservation equation for the species of gas phase in PC is given by:

$$\rho_g \varepsilon_{PC}\frac{\partial y}{\partial t} + \rho_g u_g \varepsilon_{PC}\frac{\partial y}{\partial x} = D\rho_g \varepsilon_{PC}\frac{\partial^2 y}{\partial x^2} + \varepsilon_{PC} w \tag{10}$$

Solid phase energy equation:

$$\rho_s c_s (1-\varepsilon_{PC})\frac{\partial T_s}{\partial t} = \lambda_e \frac{\partial^2 T_s}{\partial x^2} - \frac{\partial q_r^n}{\partial x} + h_v(T_g - T_s) \tag{11}$$

Where the local net radiative heat flux within the PC is expressed as: $q_r^{\,n}(\tau) = q_r^{\,+}(\tau) + q_r^{\,-}(\tau)$,

$$q_r^+(\tau) = 2\pi\left[\begin{array}{l} I_0^+(\tau_{-x_{FP}})E_3\left(\tau_{-x_{FP}}\right) \\ +\int_{\tau_{-x_{FP}}}^{\tau_{-L}} I_b(\tau')E_2(\tau')d\tau' \end{array}\right]E_3(\tau) + 2\pi\left[\int_0^{\tau} I_b(\tau')E_2(\tau-\tau')d\tau'\right], \quad (12)$$

and

$$q_r^-(\tau) = -2\pi\left[\begin{array}{l} I_0^-(\tau_{x_{PC}})E_3\left(\tau_{x_{PC}}-\tau\right) \\ +\int_{\tau}^{\tau_{x_{PC}}} I_b(\tau')E_2(\tau'-\tau)d\tau' \end{array}\right] \quad (13)$$

The optical thickness in the PC section is defined as $\tau = \kappa_{PC}(x)$. The divergence of the net radiative heat flux, $\frac{\partial q_r^n(\tau)}{\partial x}$ in Equation 11, is expressed as:

$$\frac{\partial q_r^n(\tau)}{\partial x} = -2\pi\kappa_{PC}\left[\begin{array}{l} I_0^+\left(\tau_{-x_{FP}}\right)E_3\left(\tau_{-x_{FP}}\right) \\ +\int_{\tau_{-x_{FP}}}^{\tau_{-L}} I_b(\tau')E_2(\tau')d\tau' \end{array}\right]E_2(\tau) - 2\pi\kappa_{PC}\left[\begin{array}{l} -2I_b(\tau)+I_0^-\left(\tau_{x_{PC}}\right)E_2\left(\tau_{x_{PC}}-\tau\right) \\ +\int_0^{\tau_{x_{PC}}} I_b(\tau')E_1\left(\left|\tau-\tau'\right|\right)d\tau' \end{array}\right], \quad (14)$$

where, the last term of the Equation 14 is defined as:

$$\int_0^{\tau_{x_{PC}}} I_b(\tau')E_1\left(\left|\tau-\tau'\right|\right)d\tau' = \int_0^{\tau} I_b(\tau')E_1(\tau-\tau')d\tau' + \int_{\tau}^{\tau_{x_{PC}}} I_b(\tau')E_1(\tau'-\tau)d\tau'$$

In the air jacket, heat transfer from the hot gas in PC to the wall is assumed to be equal to heat convection from the wall to the combustion air in the air jacket. This amount of heat is used to increase in the sensible heat of the air flowing in the air jacket. Thus, we obtain:

$$\int_0^{x_{PC}} U_w\left(T_g - T_w\right)\left(2\pi r_{PC}\right)dx = h_w A_w \Delta T_{ln} \quad (15)$$

$$\dot{m}_a c_a dT_a = h_w\left(T_w - T_a\right)dA \quad (16)$$

$$\Delta T_{ln} = \frac{T_{ai} - T_{ao}}{\ln\left[\frac{T_w - T_{ao}}{T_w - T_{ai}}\right]}$$

where

and the air inlet temperature T_{ai} is considered to be equal to ambient temperature.

The T_{ao} as a function of T_w and T_{ai},can be find by integrating Equation 16 over the surface area of the wall. By substituting T_{ao} into Equation 15 gives the following equation,

$$T_w = \frac{C\int_0^{x_{PC}} T_g(x)dx + (B-1)T_{ai}}{D},$$

where B, C, and D are defined as

$$B = \exp\left(-2\pi r_{PC}x_{PC}h_w / \dot{m}_a c_a\right),$$

$$C = 2\pi r_{PC}U_w \ln B / \left(h_w A_w\right),$$

and $D = C + Bx_{PC} - 1$.

The volumetric heat transfer in FP is considered constant and is equal to 9.1×10^5 W/m^3·K [22] because the fuel flow rate is very small and the heat transfer between the fuel and solid phase is not significantly changed with varying firing rates. The continuous structure of a packed bed is assumed. The correlation for volumetric heat transfer coefficient Nu_v used in PC is given by the following correlation Wakao *et al.* [23]:

$$Nu_v = h_v d_p^2 / \lambda_g = A_{sf} d_P\left(2 + 1.1Re_{d_p}^{0.6}Pr^{1/3}\right) \quad (17)$$

where, the specific surface area and the effective thermal conductivity are defined as $A_{sf} = \frac{6(1-\varepsilon_{PC})}{d_P}$ and $\lambda_e = (1-\varepsilon_{PC})\lambda_s$ respectively. Equations 15 and 16 were used to solve. The value of nine unknowns (T_F and T_s in the FP: $\dot{m}_{mix}$, T_{mix} and T_{ao} in the mixing chamber, T_g, T_s, y and T_w in the PC) can be found.

The convergence criteria for numerical computation of all variables are set to 10^{-6}. From the preliminary calculation, the result indicated that zero heat flux boundary condition provided the nearest result with the experimental ones. Therefore, the zero heat flux boundary was used in this model and the boundary conditions are summarized in Table 1.

The initial conditions for these simulations were obtained from experimental data. The physical properties of gas, based on the average temperature at each zone of FP, a mixing chamber and PC, were assumed to be constant. All the properties used are summarized in Table 2. The conservation equations of species and energy both in FP and PC were discretized by finite differential approximations. An implicit difference scheme was adopted with respect to time, and a central difference scheme was adopted with respect to space.

Based on our preliminary experiment, the optimum condition to produce synthetic gas from small downdraft

gasification were done. The average compositions of synthetic gas from Mangium wood were measured by using the gas chromatography. The synthetic gas is mixture of 14.66% H_2, 10.50% CH_4, 9.54% CO, 13.33% CO_2, and 51.97% N_2 provide highest heating value. The mixture has high inert content of CO_2 and N_2. Therefore, the average calculated heating value of synthetic gas is very low (5842 kJ/kg). The synthetic gas is difficult to burn in conventional gas burner. Therefore, the technology of high preheating effect of the LMPB is suitable to use in this condition. The gas composition and the calculated heating value from experimental result were used as input parameter in the numerical model.

Table 1. Boundary conditions.

FP Section		PC Section	
$x = -x_{FP}$	$x = -L$	$x = 0$	$x = x_{PC}$
$T_F = T_0$	$\frac{\partial T_F}{\partial x} = 0$	$T_g = T_{mix}$	$\frac{\partial T_g}{\partial x} = 0$
$\frac{\partial T_s}{\partial x} = 0$	$\frac{\partial T_s}{\partial x} = 0$	$\frac{\partial T_s}{\partial x} = 0$	$\frac{\partial T_s}{\partial x} = 0$
-	-	$y = y_0$	$\frac{\partial y}{\partial x} = 0$
$I_0^+(\tau_{-x_{FP}}) = \frac{\sigma T_0^4}{\pi}$	$I^-(\tau_{-L}) = I_0^-(\tau_{x_{PC}})E_3(\tau_{x_{PC}}) + \int_0^{\tau_{x_{PC}}} I_b(\tau')E_2(\tau')d\tau'$	$I^+(\tau_0) = I_0^+(\tau_{-x_{FP}})E_3(\tau_{-x_{FP}}) + \int_{\tau_{-x_{FP}}}^{\tau_{-L}} I_b(\tau')E_2(\tau')d\tau'$	$I_0^-(\tau_{x_{PC}}) = \frac{\sigma T_0^4}{\pi}$

Table 2. Solid property data used for simulations.

Properties	FP	PC	Unit
Porosity, ε	0.61	0.36	-
Effective thermal conductivity of solid, λ_e	12.1	1.8	$W.m^{-1}.K^{-1}$
Volumetric heat transfer coefficient, h_v	[22]	[23]	$W.m^{-3}.K^{-1}$
Absorption coefficient, κ	1750	71	m^{-1}
Apparent density, $\rho_s(1-\varepsilon)$	2510	1714	kg/m^3
Specific heat, c_s	3120	775	$J.kg^{-1}.K^{-1}$

3. RESULTS AND DISCUSSION

In the section the fluid and solid temperature profiles were predicted to investigate the thermal structure of the system and the burner performance. The final error in the global energy balance of numerical results was less than 1%. The following figures show thermal structure, effect of equivalence ratio, effect of firing rate and the burner performance in term of radiant output efficiency.

3.1. Thermal Structure

Figure 3 shows the gas temperature, solid temperature, product mole fraction and dimensionless reaction rate at equivalence ratio of 0.7 and firing rate of 5 kW. The FP and the PC are in contact by thermal radiation. The FP and the PC serve as a radiative heat absorber and radiative heat emitter respectively. In the FP, because of a high heat transfer between gas and solid phases, the solid temperature is slightly higher than the gas temperature and are nearly identical. Therefore, the fuel is preheated before flow through the mixing chamber. While a combustion air flow into the system at Section 4 with temperature of 25°C and is preheated by the hot wall of the PC. After that the preheated air flow in to the mixing chamber with temperature of 174°C. In the mixing chamber, the preheated air and the preheated gaseous fuel from the FP are met and mixed followed by reaction in the PC. In the PC, the reaction zone begins where the gas and solid temperatures are equal and ends where the extrapolation of the heat release rate curve crosses the x-axis. At the pre-flame zone, the solid temperature is higher than the gas phase. Therefore, heat is transfer from the solid to the incoming combustible gas mixture for preheating. After that the combustion is occurred and the gas temperature is greater than the solid temperature thus heat is transferred from the gas to the solid phase. Suddenly, the heat is recirculated from the post-flame zone to the pre-flame zone by solid to solid conduction and radiation. Because of highly preheating effect within the FP, within the PC and at the hot wall of PC, the LMPB can be used to burn the low-calorific-synthetic-gas and provide stabilizes combustion within porous medium. This is lead to the excess enthalpy combustion that provide more advantages over free flame [15], [24]-[28] occurs. The numerical shows the same trend as previous work [21], [22]. Moreover, the combustion within the PC show the same phenomenon as that of premixed porous burner of previous work.

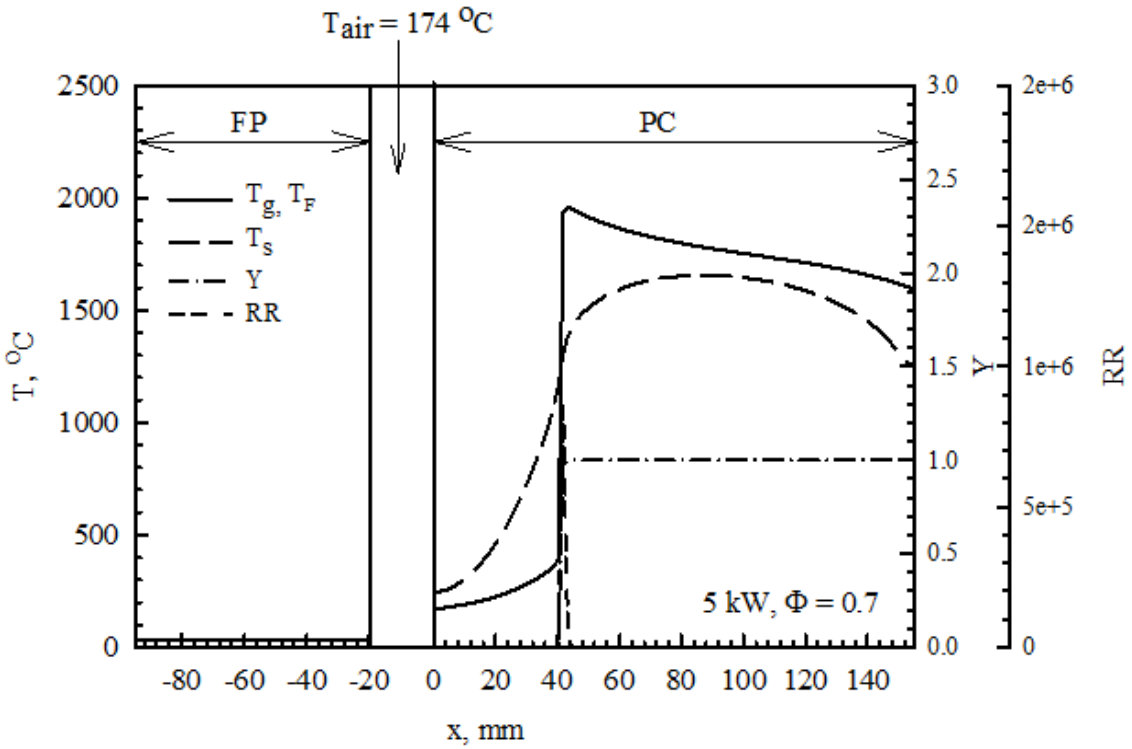

Fig. 3. The temperature profiles, product mole fraction and dimensionless reaction rate at equivalence ratio of 0.7 and firing rate of 5 kW.

3.2. Effect of Equivalence Ratio

Figure 4 presents predicted steady state temperature profiles for a range of equivalence ratio (Φ= 0.6 - 1.0) with constant firing rate at 5 kW. In this study, increasing equivalence ratio is done by decreasing air flow rate and fixing fuel flow rate. Higher average temperature in the PC are found as Φ increase, which is relate to the enrichment of the quality of mixture. Also, the reaction zone (location of the maximum gas temperature) move toward the upstream zone. On the contrary, increasing Φdoes not significantly affect the temperature in the FP, because the fuel mass flow rate does not change with varying Φ.

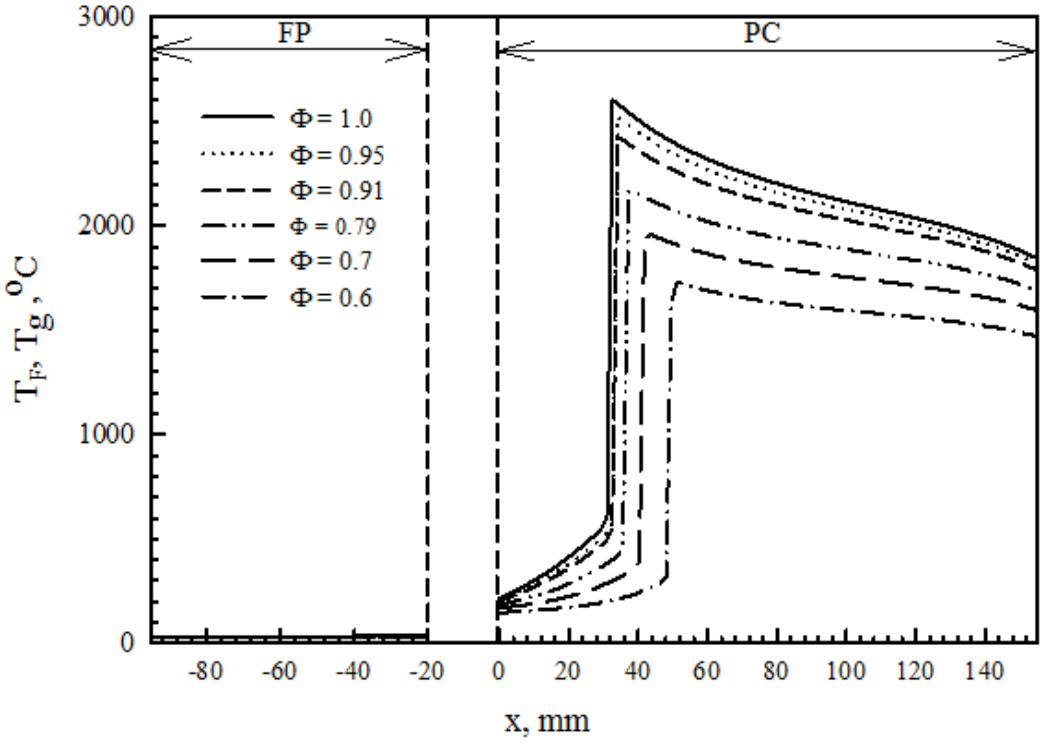

Fig. 4. Effect of equivalence ratio.

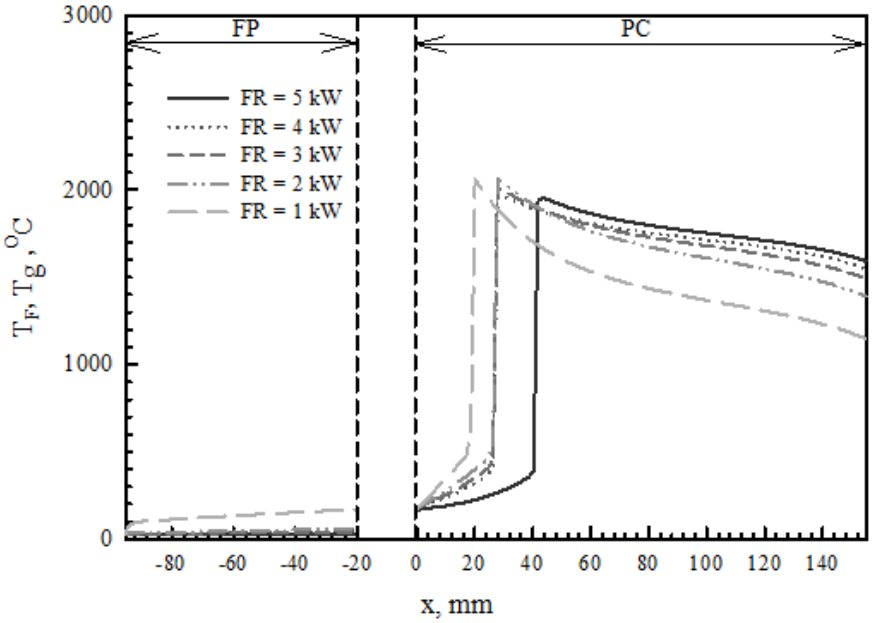

Fig.5. Effect of firing rate.

3.3. Effect of Firing Rate

Figurer 5 shows the effect of firing rate (FR) with Φ= 0.7. Increasing firing rate at a fixed Φ is done by increasing both fuel and air flow rate in constant fuel and air ratio. Increasing firing rate, the maximum temperature in the PC shows the decreasing trend, but on the other hand the temperature at the downstream zone increase. This is due to a higher convection heat transfer from the reaction zone to the post flame zone when increasing fuel and air flow rate. In the FP, the temperature is decreased with increasing firing rate because of increasing fuel mass flow rate.

3.4. Burner Performance

The measuring of porous burners performance standard procedure is lacking. Much of the early study on porous burners reported burner performance in term of radiant output efficiency. Thus, the burner performance in term of radiant output efficiency of the LMPB in case of using low-calorific-synthetic-gas as a fuel is clarified. Figure 6 shows the burner performance at varying firing rate and equivalence ratio. The radiant output efficiency is defined as the useful energy for heating product at a downstream end [28].

$$\eta_{rad} = \frac{\text{heat radiates out the exit of the burner}}{\text{Firing rate}}. \quad (18)$$

At every firing rate the η_{rad} increased with increasing Φ because of increasing in temperature in the PC. At constant Φ, the η_{rad} is decreased with increasing FR. This is due to a large convective heat loss at the downstream end with a relatively high flow velocity.

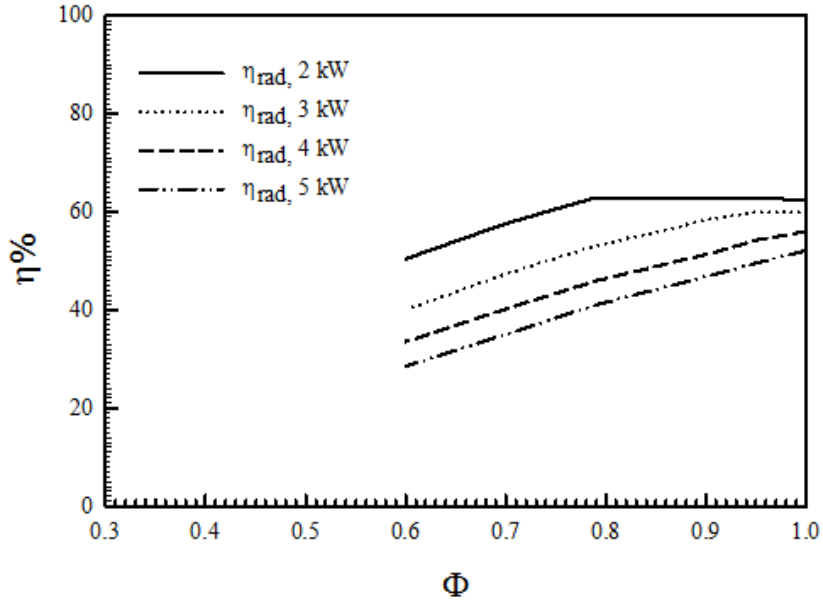

Fig. 6. Radiant output efficiency of LMPB.

4. CONCLUSIONS

The main gold of this work was to acquire the numerical results for clarifying the burner performance of LMPB in case of using low calorific synthetic-gas from biomass gasification as a fuel. A single-step global reaction, a one-dimensional model and steady state approach were considered. The gas and solid phase temperatures were calculated to investigate the effect of equivalence ratio and firing rate on thermal structure and burner performance. The following results were obtained:

[1] With increasing Φ, the temperature within the PC was increased and the reaction zone move toward to the upstream zone. Not like in the FP, Φ doses not significantly affect the temperature profiles.

[2] Increasing FR, the maximum temperature in the PC show the decreasing trend while the temperature at the downstream zone increase. In the FP, the temperature is decreased with increasing FR. At every firing rate the η_{rad} is increased with increasing Φ while the η_{rad} is decreased with increasing FR.

REFERENCES

[1] Mohammed M.A.A., Salmiaton A., Wan Azlina W.A.K.G., Mohammad Amran M.S., and Fakhru'L-Razi A., 2011. Air gasification of empty fruit bunch for hydrogen-rich gas production in a fluidized-bed reactor. *Energy Conversion and Management* 52(2): 1555-1561.

[2] Cohce M.K., Dincer I. and Rosen M.A., 2010. Thermodynamic Analysis of Hydrogen Production from Biomass Gasification. *International Journal of Hydrogen Energy* 5(10): 4970-4980.

[3] Sun Y., Li R.D., Yang T.H., Kai X.P., He Y.G., 2013. Gasification of biomass to hydrogen rich gas in fluidized beds using porous medium as bed material. I*nternational Journal of Hydrogen Energy* 38: 14208-14213.

[4] Heidenreich S. and U.P. Foscolo. 2015. New concepts in biomass gasification. *Progress in Energy and Combustion Science* 46: 72-95.

[5] Wijesinghe L.C.A.de S., 1988. Biomass fuel and its utilization in Sri Lanka. *International Energy Journal* 10(1): 67-80.

[6] Qingyu J. and H. Yuan-bin. 1999. A study of biomass as a source of energy in China. *International Energy Journal* 21(1): 1-10.

[7] Narang H.P., Parashar D.C., Bhattacharya S.C., and Abdul Salam P. 1999. A study of biomass as a source of energy in India. *International Energy Journal* 21(1): 11-23.

[8] Amur G.Q. and S.C. Bhattacharya.1999. A study of biomass as a source of energy in Pakistan. *International Energy Journal* 21(1): 25-36.

[9] Elauria J.C., Quejas R.E.T., Cabrera M.I., Liganor R.V., Bhattacharya S.C. and Predicala, N.L.J. 1999. Biomass as energy source in the Philippines. *International Energy Journal* 21(1): 37-53.

[10] Kumaradasa M.A., Bhattacharya S.C., Abdul Salam P., Amur G.Q., 1999. A Study of biomass as a source of energy in Sri Lanka. *International Energy Journal* 21(1): 55-68.

[11] Khoa T.M., Bhattacharya S.C., and Amur G.Q. 1999. A study of biomass as a source of energy in Vietnam. *International Energy Journal* 21(1): 69-75.

[12] Hardesty D.R. and F.J. Weinberg. 1974. Burner producing large excess enthalpies. *Combustion Science and Technology* 8: 201-214.

[13] Jones A.R., Lloyd S.A. and Weinberg F.J., 1978. Combustion in heat exchangers. *Proceeding of the Royal Society a Mathematical, Physical and Engineering Sciences* 360: 97–115.

[14] Al-Hamamre Z., Diezinger S., Talukdar P., Von Issendorff F. and Trimis D., 2006. Combustion of low calorific gases from landfills and waste pyrolysis using porous medium burner technology. *Process Safety and Environmental Protection* 84 (4): 297-380.

[15] Wood S. and A.T. Harris. 2008. Porous burners for lean-burn applications. *Progress in Energy and Combustion Science* 34: 667–684.

[16] Alavandi S.K. and A.K. Agrawal 2008. Experimental study of combustion of hydrogen–syngas/methane fuel mixtures in a porous burner. *International Journal of Hydrogen Energy* 33(4), 1407–1415.

[17] Francisco Jr., R.W., Costa M., Catapan R.C. and Oliveira A.A., 2013. Combustion of hydrogen rich gaseous fuels with low calorific value in a porous burner placed in a confined heated environment. *Experimental Thermal and Fluid Science* 45: 102–109.

[18] Al-attab K.A., Chung Ho J. and Zainal Z.A., 2015. Experimental investigation of submerged flame in packed bed porous media burner fueled by low heating value producer gas. *Experimental Thermal and Fluid Science* 62: 1-8.

[19] Wongwatcharaphon K. and K. Theinnoi. 2013. Effect of physical properties of porous combustor on radiant output and fuel-preheated efficiency of a non-sprayed porous burner. *Applied Mechanics and Materials* 421: 819-825.

[20] Wongwatcharaphon K., Tongtem P. and Jugjai S., 2009. Highly preheated fuel and air in nonpremixed porous burner. In *World Renewable Energy Congress 2009 – Asia The 3rd International Conference on "Sustainable Energy and Environment (SEE 2009)"* 18-23 May 2009, Bangkok, Thailand.

[21] Wongwatcharaphon K., Tongtem P. and Jugjai S., 2013. Numerical and experimental study of late mixing porous burner. *Journal of the Energy Institute* 86(1): 15-23.

[22] Yoshizawa Y., Asaki K., Echigo R., 1988. Analytical study of the structure of radiation controlled flame. *International Journal of Heat and Mass Transfer* 31: 311-319.

[23] Wakao N., Kaguei S., and Funazkri T., 1979. Effect of fluid dispersion coefficients on particle-to fluid heat transfer coefficients in packed beds: Correlation of Nusselt numbers. *Chemical Engineering Science* 34: 325-336.

[24] Howell J.R., Hall M.J. and Ellzey J.L., 1996. Combustion of hydrocarbon fuels within porous inert media. *Progress in Energy and Combustion Science* 22(2): 121–145.

[25] Trimis D. and F. Durst. 1996. Combustion in a porous medium – advances and applications. *Combustion Science and Technology* 121(1–6): 153–168.

[26] Mejeebu M.A., Abdullah M.Z., Bakar M.Z.A., Mohamad A.A., Muhad R.M.N and Abdullah M.K., 2009. Combustion in porous media and its application- a comprehensive survey. *Journal of Environmental Management* 90: 2287-2312.

[27] Brenner G., Pickenäcker K., Pickenäcker O., Trimis D., Wawrzinek K. and Weber T., 2000. Numerical and experimental investigation of matrix-stabilized methane/air combustion in porous inert media. *Combustion and Flame* 123: 201-213.

[28] Barra A.J. and L.J. Ellzey. 2004. Heat recirculation and heat transfer in porous burners. *Combustion and Flame* 137: 230–241.

NOMENCLATURE

A = area (m^2), frequency factor of combustion (s^{-1})
B = dummy variable
c = specific heat (J/kg.K)
C = dummy variable
FR = firing rate (kW)
d_P = diameter of particle (m)
D = diffusion coefficient (m^2/s), dummy variable
E = activation energy (kJ/mol)
E_n = exponential integral function
h = enthalpy (J/kg)
h_o = heat of reaction (J/m^3)
h_v = volumetric heat transfer coefficient ($W/m^3.K$)
H = local net radiative heat flux (-)
I = incident radiation (W/m^2)
L = length of mixing chamber (m)
$\dot{m}$ = mass flow rate (kg/s)
Nu = Nusselt number
Pr = Prandtl number
q_r = radiation flux (W/m^2)
r = radius (m)
R = gas constant (J/mol.K)
Re = Reynolds number
t = time (s)
T = temperature (K, ^oC)
u = interstitial gas velocity (m/s)
U = overall heat transfer coefficient ($W/m^2.K$)
V = volume (m^3)
w = reaction rate (1/s)
x = coordinate system (m)
y = product mole fraction
α = wall area to volume ratio (m^2/m^3)
ε = porosity
Φ = equivalence ratio
κ = absorption coefficient (m^{-1})
λ = thermal conductivity (W/m.K)
λ_e = effective thermal conductivity (W/m.K)
ρ = density (kg/m^3)
σ = Stefan – Boltzmann constant ($W/m^2.K^4$)
τ = optical thickness = κ x

Superscripts

\+ = positive direction
\- = negative direction
n = net

Subscripts

0 = ambient
a = air
ai = air inlet of air jacket
ao = air outlet of air jacket
ad = adiabatic
b = black body
F = fuel
FP = fuel-preheating porous medium
g = gas
mix = mixture
v = volumetric
w = wall
p = particle
PC = porous combustor
s = solid